Ferroelectricity and multiferroic quantum critical behaviors in $Co_2V_2O_7$

R. Chen [1,3,*] H. J. Hu [1] Q. K. Lei [1] C. B. Liu [2,†] C. Dong [3] X. Y. Yue [4] Z. Qu [1] H. W. Wang [3] Y. Qiu [1] D. Chen [1] X. L. Yi [1] Z. W. Ouyang [3] and J. F. Wang [3]

[1] *College of Physics and Electronic Engineering, Xinyang Normal University, Xinyang 464000, China*
[2] *College of Physics and Electronic Engineering, Nanyang Normal University, Nanyang 473061, China*
[3] *Wuhan National High Magnetic Field Center, Huazhong University of Science and Technology, Wuhan 430074, China*
[4] *Institute of Physical Science and Information Technology, Anhui University, Hefei 230601, China*

(Received 14 May 2023; accepted 16 November 2023; published 4 December 2023)

We present isothermal ferroelectric (FE) and quasiadiabatic phase diagrams for single-crystal $Co_2V_2O_7$ with magnetic fields (H) along the c axis, obtained through magnetization, polarization (P), and magnetocaloric effect measurements under pulsed magnetic fields up to 30 T. The FE diagram reveals two FE phases, denoted as FE-I and FE-II, with overlapping boundaries at low temperatures (T). At 2 K, the P signal along c exhibits a positive value in FE-I, transitioning to a negative value in FE-II with increasing H. During the descending-H process, P reverses, with FE-II displaying positive polarization and FE-I displaying negative, indicative of dynamic ferroelectric behavior. Above 3 K, a paraelectric (PE) phase emerges, effectively separating the two FE phases. This PE phase correlates with the 1/2 plateau observed in the magnetization curve. Simultaneously, as T increases, the negative P signals of FE-I and FE-II sequentially reverse to positive, leading to the gradual diminishment of the signal reversal of P along the c axis due to the history of H sweeping. The magnetic Grüneisen parameter diverges near the field on both sides of the 1/2 plateau, providing evidence of multiferroic quantum criticality. Employing symmetry analysis, we propose a chiral "water-strider" type spin configuration to elucidate the origin of ferroelectricity and the magnetization process. The high-field FE phase may be associated with the quintuplet excitation of the Co1 dimer in the presence of magnetic fields.

DOI: 10.1103/PhysRevB.108.224405

I. INTRODUCTION

Multiferroic materials, particularly type II ones, are of great interest in condensed-matter physics due to their potential application of intrinsic cross magnetoelectric effects. Abundant theoretical and experimental research on the subject has proliferated over the past decades [1]. A consensus is that the ferroelectric polarization for the type II originates from the special spin orderings in compounds. Corresponding theoretical mechanisms such as symmetric exchange striction ($\boldsymbol{P} \propto \mathbf{S}_i \cdot \boldsymbol{S}_j$) [2,3], inverse Dzyaloshinskii-Moriya interaction or spin current theory [$\boldsymbol{P} \propto \boldsymbol{e}_{ij} \times (\mathbf{S}_i \times \boldsymbol{S}_j)$] [4,5], and spin dependent $d-p$ hybridization ($\boldsymbol{P} \propto \mathbf{S}_i \times \boldsymbol{S}_j \parallel \boldsymbol{e}_{ij}$) [6,7] have been proposed successively. However, there have been occasional controversies over the applicability of these mechanisms in different systems [8–11]. To solve these problems and achieve a unifying theory that includes multiferroicity, superconductivity, and other exotic phenomena, cross research between quantum magnetism and multiferroicity has gradually emerged as a hot topic [12–14]. For instance, the quantum critical behaviors in doped $SrTiO_3$ are regarded as the origin of its superconductivity [15], which is closely related to their dynamic ferroelectricity [16,17]. Particular spin configurations or orders induced improper ferroelectricity, skyrmion texture and Bose-Einstein condensation phenomena are summarized to propose advanced concepts such as ferroelectric and multiferroic quantum criticality [18,19], dynamic multiferroicity [13,20,21], etc.

Recently, a low-dimensional spin system $T_2V_2O_7$ ($T =$ Ni, Co) has been discovered [22–24]. This system possesses multiple metamagnetic phase transitions and abnormal electric polarization switches, and the field-induced ferroelectric phases are distributed on both sides of the 1/2 and 3/4 quantum magnetization plateaus, which may be related to the condensed state of the magneton. The compounds crystallize in a monoclinic structure with the space group of $P2_1/c$. The magnetic ions, Ni^{2+} or Co^{2+}, form two types of edge-sharing octahedra that compose bond-alternating skew chains along the c axis as shown in the inset of Fig. 1(a). High-field magnetization up to 120 T reveals an underlying "dimer+monomer" spin configuration and possible supersolid phases in $Ni_2V_2O_7$ [25]. What is even more intriguing are the successive field-induced polarization reversals and flop behaviors, along with its anisotropic quantum magnetization plateau in $Co_2V_2O_7$ [26]. In particular, a 1/2 magnetization plateau is observed after a spin-flop phase transition within 5.4–11.6 T, followed by a 3/4-like plateau at 15.7 T, when the field is applied along the b axis. For both a and c axes, only two anomalies in $M(H)$ are observed, signaling the existence of a 1/2-like magnetization plateau, as illustrated in Fig. 1(a). Those complex anisotropic magnetic and multiferroic phases inevitably contain rich physics, making the system a typical candidate for studying dynamic multiferroicity with quantum criticality.

*chenrui@xynu.edu.cn
†congbinliu2020@163.com

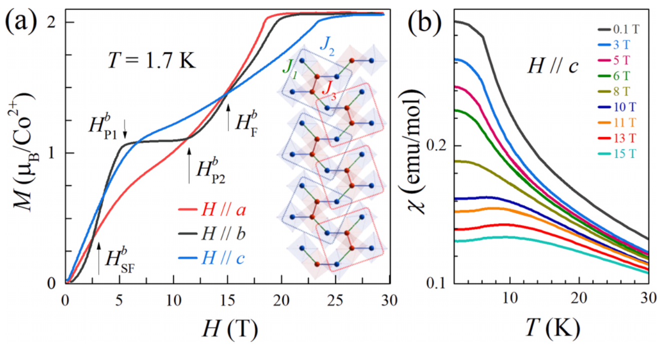

FIG. 1. (a) High-field $M(H)$ curves for three crystalline axes measured at 1.7 K reported in Ref. [33]. The inset is the crystal structure of $Co_2V_2O_7$ viewed along the a axis. The red and blue spheres denote the Co1 and Co2 atoms, respectively. (b) Magnetic susceptibility for $H \parallel c$ under different field strengths up to 15 T.

Motivated by these considerations, the reinvestigation of $Co_2V_2O_7$ is carried out in this work. It is worth noting that the previous studies mainly focused on the b axis. Significant magnetization plateaus and ferroelectric (FE) phases have been observed along the b axis. However, we recognized untapped potential in examining P reversals induced by ascending and descending magnetic fields along the c axis. This exploration promises insights into dynamic multiferroicity and opens up a spectrum of possibilities. To unravel the underlying physics, we have employed high-field magnetization, electric polarization, and magnetocaloric effect measurement techniques mainly for the c axis, and constructed the magnetoelectric phase diagrams under isothermal and quasiadiabatic environments. Clearly defined multiferroic quantum critical phase boundaries and critical points have been experimentally observed. The P along the c axis exhibits reversible positive-to-negative or negative-to-positive phenomena at the finite low temperature in different field-sweep histories, demonstrating dynamic multiferroic behavior, which can be modulated by parameters such as T, H, or the sweeping direction of H.

II. EXPERIMENTAL DETAILS

Single crystals of $Co_2V_2O_7$ were grown by a flux method. Details of crystal growth and characterization can be found elsewhere [27,28]. Magnetic susceptibility ($\chi = M/H$) was measured during warming in different magnetic fields within a physical property measurement system (PPMS). High-field experiments involving magnetization, polarization, and magnetocaloric effects were performed at the Wuhan National High Magnetic Field Center (WHMFC), utilizing pulsed high magnetic fields up to 30 T. The pulsed magnetic fields were generated by using a 10.5 ms short-pulse magnet and the high-field $M(H)$ was detected by a standard inductive method using a well-compensated pickup coil. The pulsed high-field polarization was achieved by integrating the magnetoelectric current dP/dt over time, which was detected by observing the voltage change across a series-connected shunt resistor (10 KΩ) in the measurement circuit [29–31]. In the P measurements, we applied and maintained a bias electric field of $E = 650$ kV/m to achieve complete polarization of the ferroelectric (FE) domains induced by the magnetic field. The change in electric polarization $\Delta P(H) = P(H) - P(H = 0)$ is obtained by numerically integrating dP/dt. For the magnetocaloric effect experiments, a chip thermistor made of RuO_2 was employed to determine changes in temperature for the sample by measuring the resistance using standard ac lock-in techniques. Further details on the MCE measurement methodology can be found in Ref. [32].

III. RESULTS AND DISCUSSIONS

A. High-field magnetization and polarization

Figure 1(a) shows the $M(H)$ curves of a single crystal $Co_2V_2O_7$ under pulsed high magnetic field. Before saturation, the a and c axes exhibit similar magnetization anomalies, which are distinct from the behavior observed for the b axis. In the latter case, full spin polarization is achieved after undergoing several processes including spin-flop transition (H^b_{SF}), half (H^b_{P1}, H^b_{P2}), and 3/4 (H^b_F) magnetization plateaus [26,33]. When $H < H^b_{P1}$, the $M(H)$ of $H \parallel c$ and $H \parallel a$ do not exhibit significant phase transition anomalies. For $H \parallel c$, the inflection point of the $M(H)$ curve, which is a potential phase transition signal, is close to H^b_{P1}, corresponding to the starting point of the 1/2 plateau for the b axis. Above H^b_{P1}, the M eventually saturates, with the slope of the $M(H)$ curve gradually increasing as the field increases, implying complex and possibly competitive interactions for $H \parallel c$. Figure 1(b) shows the $\chi(T)$ curves of $H \parallel c$. At 0.1 T, the χ shows an increase during cooling, gradually forming an antiferromagnetic anomaly. As the H is increased, this anomaly shifts towards lower temperatures below 8 T, which is in line with expectations for ordinary antiferromagnets. However, with further increase in H, a broad antiferromagnetic peak emerges, exhibiting a tendency towards higher temperatures within a limited range of H (10 T to 15 T), as evident from the $\chi(T)$ curves. Additionally, the χ values appear to approach a stable value at low temperatures in these fields. The anomalous evolution of the antiferromagnetic peaks suggests that the compound may adopt a distinct magnetic ordering state under low-T conditions and within a restricted range of magnetic field intensities.

Figure 2 shows the results of high-field magnetization and the change in polarization, $\Delta P(H)$, measured at temperatures near 2 K and 4.2 K. The $M(H)$ curves in Fig. 2(a) are adjusted by subtracting the Van Vleck effect as described in Ref. [33]. It can be observed that the $M(H)$ curve of 4.2 K exhibits a linear region with a small slope in the middle magnetic field ranges while H increases. Two obvious inflection points, defined as H^c_{P1} and H^c_{P2}, can be observed through its differential curve as shown in the lower right area of Fig. 2(a). By analyzing the linear region of the epitaxial curve as shown by the black dashed lines, we find that the saturation magnetization of 4.2 K is $\sim 1.5\,\mu_B/Co^{2+}$ and the middle linear region is $\sim 0.8\,\mu_B/Co^{2+}$. The ratio of the two values is close to a half, indicating that a 1/2 magnetization plateau occurs in the field region between H^c_{P1} and H^c_{P2}. However, this phenomenon cannot be observed in both $M(H)$ and its differential curve dM/dH at 1.7 K. These observations imply the relatively intricate nature of the magnetic

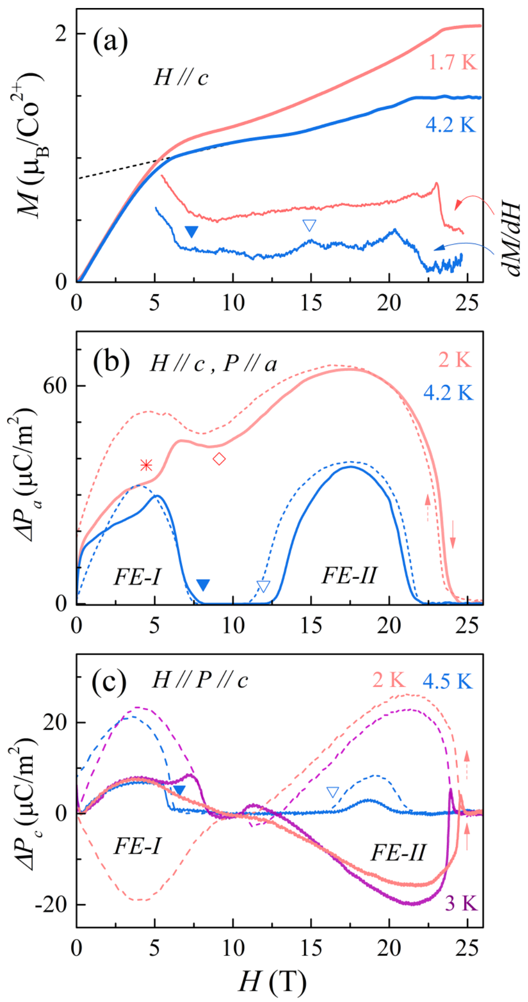

FIG. 2. (a) High-field magnetization processes of $Co_2V_2O_7$ measured at 1.7 K and 4.2 K for $H \parallel c$. The insets in the lower right area are the corresponding dM/dH curves. The symbols represent the different phase transition critical fields marked as $H_{\rm P}^c(\diamond)$, $H_{\rm P1}^c(\blacktriangledown)$, $H_{\rm P2}^c(\triangledown)$, and $H_{\rm F}^c(*)$, respectively. (b) The H dependence of electric polarization along the a axis, ΔPa, for $H \parallel c$ at 2 K and 4.2 K. (c) The H dependence of electric polarization along the c axis, ΔPc, for $H \parallel c$ at 2 K, 3 K, and 4.5 K. The solid (dashed) curve denotes the field-ascending (descending) sweep, also as seen by the solid (dashed) arrow.

interactions within $Co_2V_2O_7$, which can be modulated by thermal effects and magnetic fields. The increase of temperature enhances the thermal fluctuations, which, to some extent, suppress the strong exchange interaction between spins leading to a new equilibrium. When subjected to a finite magnetic field along the c axis, the phenomenon of a 1/2 quantum plateau occurs.

Figures 2(b) and 2(c) show the polarization $P \parallel a$ and $P \parallel c$ in the pulsed high magnetic fields. As shown in Fig. 2(b), the $\Delta P_a(H)$ curve appears as two broad bulges with the increase of $H \parallel a$ at 4.2 K, similar to a camel's bimodal. The bulges are divided into two regions—the ferroelectric phase-I (FE-I) and the ferroelectric phase-II (FE-II), by a paraelectric (PE) phase with the critical fields of $H_{\rm P1}^c$ and $H_{\rm P2}^c$ marked by the triangle symbols. As the temperature decreases, $H_{\rm P1}^c$ and $H_{\rm P2}^c$ gradually approach and converge near $H_{\rm P}^c$ at 2 K, as shown by the $\Delta P_a(H)$ curves, indicating the eventual merging of the two FE phases. The detailed field profiles of ΔP_a at various temperatures are shown in Fig. S1 of the Supplemental Material [34]. The disappearance of the PE phase coincides with the vanishing of the 1/2 magnetization plateau during cooling, suggesting that electric polarization is suppressed by the commensurate quantum ordering plateau. In addition, $\Delta P_a(H)$ reveals that ΔP_a exhibits good overlap in the high-field FE-II phase during both ascending and descending field sweeps, whereas the behavior differs in the low-field FE-I phase. At 2 K and $H < H_{\rm P}^c$, the curve at the asterisk position displays a concave shape during an H-ascending sweep, whereas it exhibits bulging at the same location during descent. Initially, the absence of overlap in ΔP_a of FE-I may be attributed to the presence of residual electrical domains within the sample during measurements, resulting in incomplete polarization during the ascending field process. This scenario shows similarities to domain wall pinning or depinning processes observed in distinct histories of sweeping H such as in $Ni_3V_2O_8$ [35] and $CuFeO_2$ [36]. However, this behavior persistently manifests itself across successive and multiple polarization measurements, indicating its intrinsic physical nature.

Figure 2(c) illustrates the polarization along the c axis for $H \parallel c$, $\Delta P_c(H)$, at temperatures of 2 K, 3 K, and 4.5 K. For the detailed $\Delta P_c(H)$ curves at different temperatures, please consult Fig. S2 of the Supplemental Material [34]. The $\Delta P_c(H)$ curves reveal two FE phases above 3 K, with a PE phase between them, as shown in Fig. 2(c). As the temperature decreases, gradual convergence and merging of the two FE phases are observed, reminiscent of ΔP_a. Notably, distinctive reversal phenomena are observed in the polarization signals of FE-I and FE-II in $\Delta P_c(H)$. Particularly noteworthy is the complete reversal of polarization behavior at 2 K exhibited by the $\Delta P_c(H)$ curves for $H \parallel P \parallel c$ in both ascending and descending H sweeps. The following summarizes some detailed features. (1) There is only one FE phase, FE-I, at 5 K. When the temperature drops to 4.5 K, both signals of ΔP_c in FE-I and FE-II phases exhibit positive values. Additionally, the ΔP_c in the descending field surpasses that in the ascending field, implying the existence of hysteresis in the polarization during the descending- and ascending-H processes. (2) When the temperature is lowered to 3 K, the signal of ΔP_c in the FE-I phase demonstrates a positive value, whereas the signal in the FE-II phase exhibits a negative value during the process of magnetic field ascent. This behavior suggests that an H induces a reversal of P. However, during the descent of H, the signal in the FE-II phase becomes positive, while the ΔP_c in FE-I remains unchanged, signifying that another type of polarization reversal occurs when subjected to different scanning directions in the ascending and descending fields. (3) For further temperature reduction to 2 K, during the field increase process, the signal of ΔP_c in the FE-I phase is positive, but the signal in the FE-II phase becomes negative. During the field descent, the signal in the FE-II phase becomes positive first, followed by the signal in the FE-I phase becoming negative. These observations confirm that the system exhibits both field-induced P reversal from FE-I to FE-II and P reversal due to the sweep history of H, i.e., H ascending and descending. In addition, cooling can also cause P reversal phenomenon in the system [22]. This is an instance

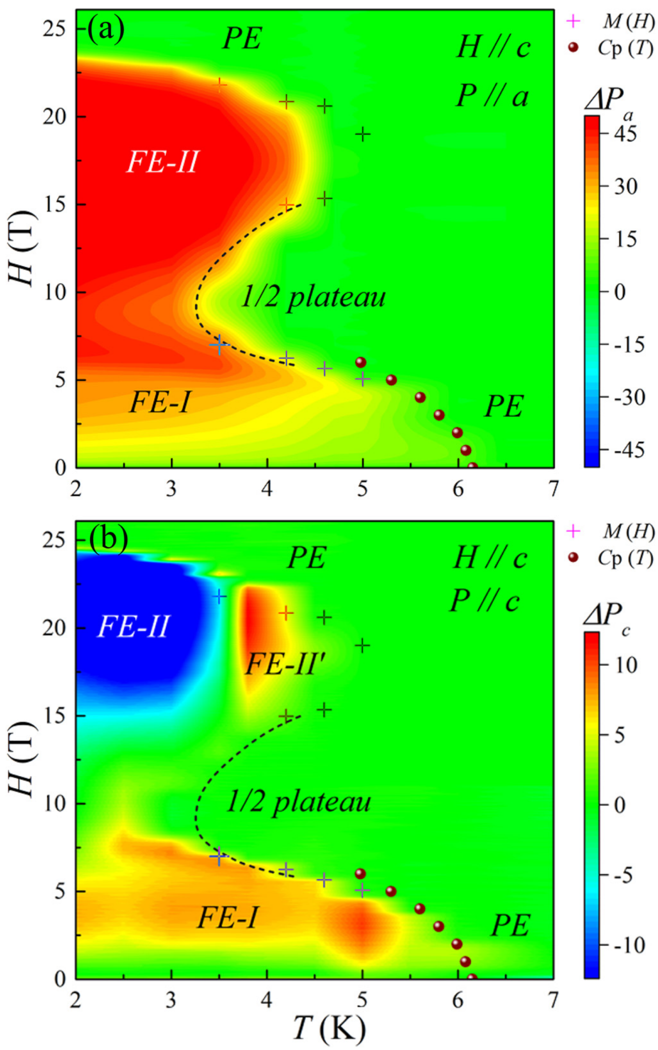

FIG. 3. H-T phase diagrams of (a) $P\|a$ and (b) $P\|c$ for $H\|c$ mapped by plotting the strength of polarization using $\Delta P(H)$ curves for H ascending at different temperatures. The symbols denote the phase-transition points extracted from magnetization and specific heat $C_p(T)$ curves. Dashed lines are provided as guides for the eye.

of such a phenomenon occurring concurrently within the same sample.

To facilitate further research, we have established FE mapping H-T phase diagrams for $P \parallel a$ and $P \parallel c$ using detailed polarization data obtained during ascending field sweeps along the c axis. These diagrams are depicted in Fig. 3. At low temperatures ($T < 3$ K), it is apparent that the FE-I and FE-II phases of $H \parallel c$ exhibit a partial overlap, while the PE phase, formed by the 1/2 plateau state at relatively higher temperatures, serves as a separator between them. With the temperature increasing, the high-field FE-II phase ceases to exist at approximately 5 K, whereas the low-field FE-I phase gradually diminishes above 6.5 K. The polarization reversal between FE-I and FE-II, as well as the T-dependent polarization inversion behavior in FE-II, are also clearly depicted in Fig. 3(b).

To gain insight into the intricate quantum magnetism and polarization reversal phenomena in $Co_2V_2O_7$, our study considered the zero-field magnetic structure [37] and took into account considerations of symmetry and spin-orbit coupling effects to predict the spin configuration of each phase under an applied magnetic field. Three superexchange interactions can be obtained based on the different distances between magnetic atoms, represented by bond length as two next nearest neighbors ($J_1 = 3.033$ Å, $J_2 = 3.053$ Å) and one nearest neighbor interaction ($J_3 = 2.97$ Å). Previous studies have regarded the compound system as the magnetic chains along the c direction from a structural perspective [23,37], where adjacent magnetic chains are linked through the nearest neighbor interaction J_3. However, the non-negligible nature of J_3 poses difficulties when analyzing physical problems and conducting theoretical calculations [23,33]. Recently, Matsuda *et al.* studied the magnetization behavior of $Ni_2V_2O_7$ using a superhigh magnetic field up to 120 T and proposed a theoretical explanation model involving "dimer+monomer" configuration, which enhanced our understanding of the material system [25]. On the basis of this research result, we conducted further analysis of $Co_2V_2O_7$. The material has a space group of $P2_1/c$ and its symmetry principal axis is the b axis. Considering the two atoms Co1 close to each other as dimers, the magnetic structural units in this compound comprise one dimeric body connected to four neighboring monomer Co2 atoms, resembling a water strider. This configuration is depicted within the blue or dashed boxes in Figs. 1(a) and 4(a). Along the b direction, two water stride units with different orientations are connected alternately by their left and right legs, giving rise to a chiral structure along the b axis, as depicted in Fig. 4(a). According to the figures, the smallest translational symmetric unit consists of adjacent water strider, i.e. the red and blue boxes in Fig. 1(a), together containing eight atoms. Of these atoms, five are internal, while the remaining six between adjacent units are statistically treated as contributing 1/2. Thus an eight-spin system, with chiral-symmetric water striders units, is constructed for explaining the magnetization and electric polarization behavior of $Co_2V_2O_7$ combined with the spin current theory.

Figure 4(a) illustrates spatial arrangement of units in a water-strider configuration, where two skew chains are formed and distributed on both sides of the b axis. These chains can be classified as chiral left (Learus) and chiral right (Dexter), labeled with light red and light blue backgrounds, respectively. By deriving the spin-connected wave vectors e_{ij} from both chains and subsequently applying a translational symmetry operation, perfectly symmetrical left and right parts can be generated along the b mirror surface as shown in the bottom of Fig. 4(a). The application of a magnetic field to this chiral symmetric mode offers a more precise elucidation of the processes of magnetization and polarization in $Co_2V_2O_7$. Figures 4(b)–4(f) present the proposed spin evolution in different states. The analysis of powder neutron diffraction reveals that the primary antiferromagnetic spins in $Co_2V_2O_7$ are predominantly arranged on the (bc) plane under zero-field conditions [37]. When an applied magnetic field $H \parallel b$ is present, the material exhibits three FE phases (FE$_b$-I, FE$_b$-II, FE$_b$-III) and one PE phase (1/2 plateau) [26,33]. As the magnetic field increases, only the monomer in the FE$_b$-I phase experiences spin variations, leading to the disruption of glide symmetry and the generation of an electric

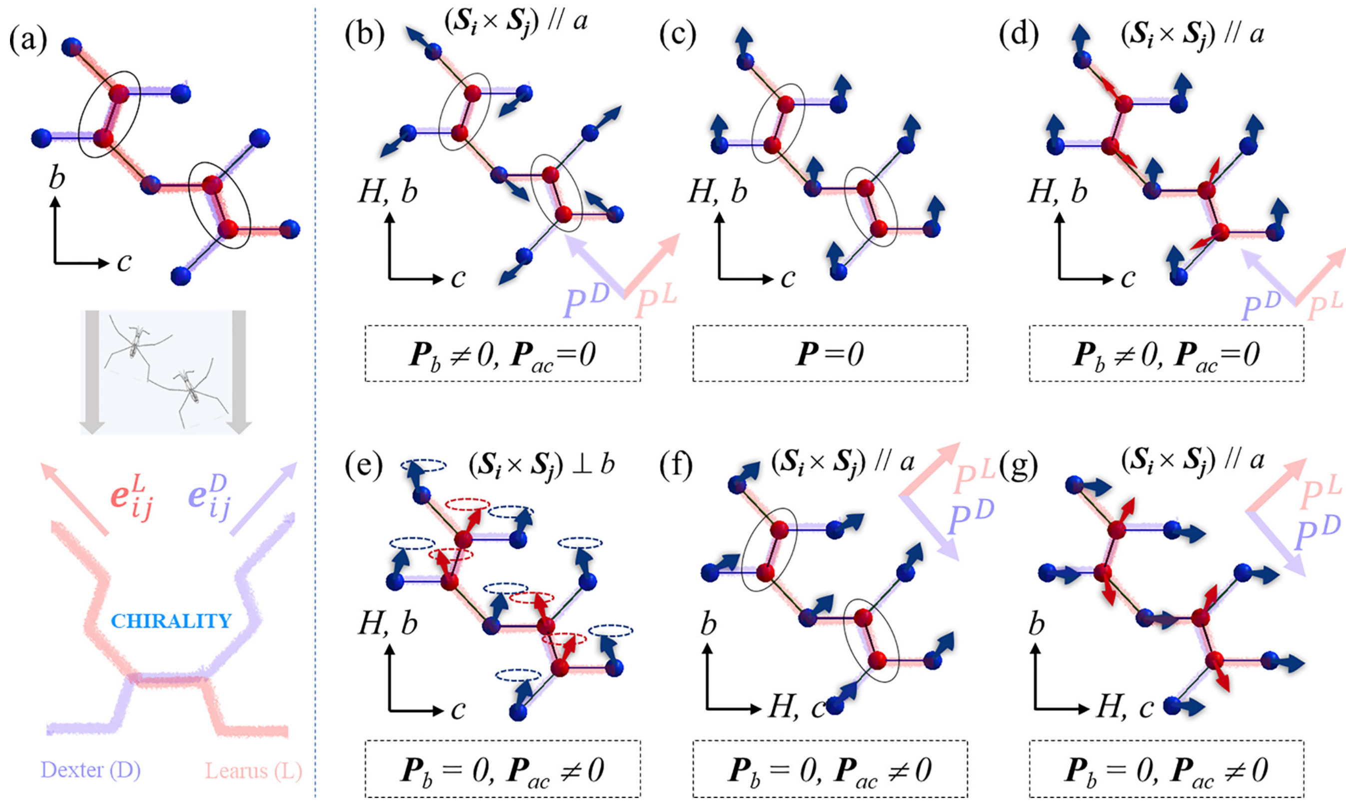

FIG. 4. (a) Arrangement of magnetic Co atoms at two sites resembles "water strider" structure, with alternating links in the form of dimers (red spheres, Co1) and monomers (blue spheres, Co2). The resulting water striders exhibit helical symmetry and form chiral chains by interconnected feet that helical symmetrically along the b direction. The bottom is a simplified representation of the chiral symmetric chains, in which the spin propagation vectors of the left-hand (L) and right-hand (D) chains are derived and translated along the b axis. (b)–(g) The spin configurations proposed in different states. (b) $H \parallel b$, $\Delta P \parallel b$ in FE_b-I state; (c) $H \parallel b$, 1/2 magnetization plateau phase; (d) $H \parallel b$, $\Delta P \parallel b$ in FE_b-II state; (e) $H \parallel b$, $\Delta P \parallel (ac)$ in FE_b-III state; (f) $H \parallel c$, $\Delta P \parallel (ac)$ in FE-I state; (g) $H \parallel c$, $\Delta P \parallel (ac)$ in FE-II state

polarization along the b direction. In the 1/2 plateau phase, four effective monomer spins become fully polarized, resulting in a PE quantum magnetization state with a configuration of spins (↑↓↑↓↑↑↑↑). Subsequently, the dimers in the FE_b-II phase begin to break under the influence of a higher magnetic field, exhibiting an electric polarization direction similar to the observed FE_b-I phase. As the spins progressively align with the direction of H, a twofold helical symmetry is disrupted, leading to the FE_b-III phase with an electric polarization in the (ac) plane. This water-strider spin image can provide a qualitative explanation for the magnetization and electric polarization reversal observed for $H \parallel c$.

In $Co_2V_2O_7$, the magnetization exhibits a plateau state at 4.2 K, but not at 1.7 K. We propose that the difference in this behavior is due to variations in the interactions between the dimer and monomer (J_1 and J_2), as well as within the dimer (J_3), which changes with temperature. At 1.7 K, the correlations of these three interactions are relatively strong. When the magnetic field completely aligns the monomers, it is strong enough to cause a break in the bonds within the dimers, resulting in only a bend in the middle magnetic field region (∼8 T) of the magnetization curve. As the T increases, thermal fluctuations enhance, leading to a relatively stronger J_3 interaction and Co1 dimerization. Consequently, applying an external H can drive the system into a quantum state similar to the observed 1/2 magnetization plateau at low temperatures for $H \parallel b$. This behavior represents a quantum critical phenomenon, with the vanishing point of the plateau corresponding to the multiferroic quantum critical point. Throughout the magnetization process, only chiral vector $[(S_i \times S_j) \parallel a]$ produces a nonzero polarization in the system. The positive and negative polarizations along the b axis cancel out each other due to the mirror symmetrical e_{ij}^L and e_{ij}^D as shown in Figs. 4(f) and 4(g). As a result, the macroscopic polarization appears in the (ac) plane for the two FE phases with $H \parallel c$. The unique water-strider structure can be attributed to the polarization reversal behavior of $H \parallel P \parallel c$ at low T. The direction of P is determined by vector $(S_i \times S_j)$ and the chirality (left-hand or right-hand) of the spin chain. It is worth noting that changes in the P signal can occur during different sweep-field histories, depending on whether the chains are arranged as e_{ij}^L or e_{ij}^D. From this special water-strider model, we speculate that, when H is applied along a specific chiral chain in $Co_2V_2O_7$, a wider 1/2 magnetization plateau and more intense FE phases occur. The appearance of an angle-dependent electric polarization signal from b to c direction at a 30° angle provides important evidence [26], with a strong value of $P \parallel b$ in the low-field FE phase and $P \parallel c$ in the high-field FE-II phase. Furthermore, the physical phenomena observed in $Co_2V_2O_7$ indicate that multiferroic quantum

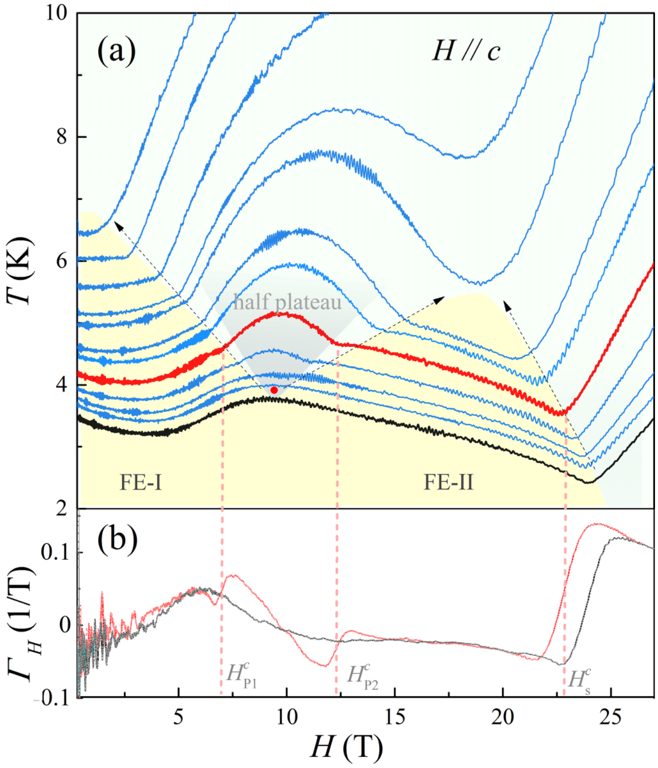

FIG. 5. (a) Magnetocaloric effect in $Co_2V_2O_7$ measured at various initial temperatures in pulsed magnetic fields ($H \parallel c$). The red symbol denotes the multiferroic quantum critical point (QCP). Gray shadow shows the half magnetization plateau evolved from QCP. The light yellow and light blue backgrounds represent FE and PE phases, respectively. The dashed arrows are the evolution of phase transition points provided as guides for the eye and separate the half plateau in magnetization, FE-II, and PM phases. (b) Magnetic Grüneisen parameter obtained from the MCE curves. The color of curves corresponds to that in (a).

critical points can be achieved by manipulating temperature, angle, and magnetic field.

B. High-field magnetocaloric effects

Figure 5(a) shows the results of magnetocaloric effect measurements at different initial temperatures under pulsed magnetic fields. Note that MCE measurements are performed under quasiadiabatic conditions during fast changing field pulses, which enables the detection of magnetic entropy changes occurring within the sample, unlike magnetization and electric polarization measurements conducted under isothermal conditions. In the provided figure, it can be observed that, at an initial temperature of 3.5 K, the $T(H)$ exhibits intriguing behavior as the magnetic field increases. Initially, a significant downward trend is observed, indicating a negative magnetocaloric effect. However, after a certain point, the T of the sample gradually increases, reaching its maximum value at around 8 T. Subsequently, the T decreases again, forming a minimum point near the saturation field $H^c_{\rm S}$, followed by a rapid rise. During this process, there are two instances where the T drops, indicating a magnetic entropy reduction process and realignment of the two magnetic orders: the monomer of Co2 and the dimer of Co1. As the initial T increases, the inflection points of $T(H)$ curves display an arched feature in the middle magnetic field region, which corresponds to the PE state of the half plateau in $M(H)$. The $T(H)$ curves can be divided into four regions: FE-I, half plateau, FE-II, and the saturated ferromagnetic state, as indicated by the red curve in Fig. 5(a). Observable dips in $T(H)$ are present at $H^c_{\rm P1}$, $H^c_{\rm P2}$, and $H^c_{\rm S}$, resembling MCE phenomena observed in various quantum critical phenomena [38–40]. The phenomenon occurring between $H^c_{\rm P2}$ and $H^c_{\rm S}$ exhibits similarities with Bose-Einstein condensation (BEC) in quantum magnets [41,42]. The plateau resembles a triplet state with $S_z = 1$, while the saturated state is analogous to a quintuplet state with $S_z = 2$, consistent with the experiments' findings in $Ba_3Mn_2O_8$ [43,44]. The intermediate state, considered as a field induced BEC region, generates a significant amount of $S^{\pm}$, inducing electric polarization and increasing the magnetic entropy in FE-II. Similar ferroelectric phenomena are reported in Ref. [45]. Consequently, the vanishing point of the $1/2$ plateau phase during cooling can be identified as a multiferroic QCP.

The divergence of the magnetic Grüneisen parameter, Γ_H, at a QCP is a highly sensitive tool for investigating quantum phase transitions [46]. Γ_H exhibits a different sign on each side of the QCP, allowing for the mapping of the entropy landscape in the vicinity of the critical point. In Fig. 5(b), we present the plot of $\Gamma_H(H)$ based on the selected MCE data, utilizing the equation as follows [47]:

$$\Gamma_H(H) = -\frac{(\partial M/\partial T)_H}{C_H} = \frac{1}{T}\frac{\partial T}{\partial H}\bigg|_s.$$

For an initial T of 4.2 K, the $\Gamma_H(H)$ curve (black line) exhibits three distinct signal changes near $H^c_{\rm P1}$, $H^c_{\rm P2}$, and $H^c_{\rm S}$. However, only one significant change is observed near $H^c_{\rm S}$ for 3.5 K. The values of the prefactor G_r at each boundary field $H^c_{\rm P1}$, $H^c_{\rm P2}$, and $H^c_{\rm S}$ are seen to be divergent, supporting the proposed "monomer+dimer" model in $Co_2V_2O_7$ and providing experimental evidence for quantum boundaries, as predicted by the formula $\Gamma_H = -G_r(H - H_c)^{-1}$ [47].

IV. CONCLUSIONS

In conclusion, we have successfully constructed the c-axis H-T phase diagrams of $Co_2V_2O_7$ under isothermal and quasiadiabatic conditions by utilizing pulse field magnetization, electric polarization, and magnetocaloric effect measurements. Our investigations reveal two FE phases, denoted as FE-I and FE-II, manifesting above 3 K. The two phases are separated by a $1/2$ magnetization plateau, referred to as the PE phase and induced by heating. Additionally, with rising temperature, we observe a progressive vanishing of FE-II and FE-I. At temperatures $T < 3$ K, the two FE phases in $P \parallel a$ and $P \parallel c$ gradually converge. The signal of $P \parallel c$ undergoes a noteworthy reversal from positive to negative during the transition from FE-I to FE-II phase, driven by an increasing magnetic field. Furthermore, at low temperatures, specifically at 2 K, FE-II and FE-I exhibit polarizations of opposite directions in a descending-sweep magnetic field, underscoring the remarkable presence of dynamic ferroelectricity in $Co_2V_2O_7$. The magnetic Grüneisen parameter exhibits divergence at $H^c_{\rm P1}$, $H^c_{\rm P2}$, and

H_S^c, suggesting the existence of a quantum critical region at the phase transitions where the half plateau appears and disappears, as well as near the critical field of saturation. This behavior characterizes the boundaries of multiferroic quantum criticality. Through symmetry analysis, we propose a chiral symmetric water-strider type spin configuration, elucidating the origin of dynamic ferroelectricity and the reversal of the P signal during the magnetization process. The electric polarization observed in the FE-II phase may arise from the breaking of bonds in H-driven dimers, analogous to the quintuplet excitation.

ACKNOWLEDGMENTS

This work was supported by the National Natural Science Foundation of China (Grants No. 12104388, No. 12074135, and No. 12104351), the Natural Science Foundation of Henan (Grant No. 232300420121), the Henan Provincial Department of Science and Technology Research Project (Grant No. 222102230105), the Hubei Province Natural Science Foundation of China (Grant No. 2021CFB027), and the Nanhu Scholars Program for Young Scholars of Xinyang Normal University.

[1] S. Dong, J.-M. Liu, S.-W. Cheong, and Z. Ren, Adv. Phys. **64**, 519 (2015).
[2] N. Lee, C. Vecchini, Y. J. Choi, L. C. Chapon, A. Bombardi, P. G. Radaelli, and S.-W. Cheong, Phys. Rev. Lett. **110**, 137203 (2013).
[3] Y. Tokunaga, S. Iguchi, T. Arima, and Y. Tokura, Phys. Rev. Lett. **101**, 097205 (2008).
[4] H. Katsura, N. Nagaosa, and A. V. Balatsky, Phys. Rev. Lett. **95**, 057205 (2005).
[5] I. A. Sergienko and E. Dagotto, Phys. Rev. B **73**, 094434 (2006).
[6] T. Nakajima, Y. Tokunaga, V. Kocsis, Y. Taguchi, Y. Tokura, and T. H. Arima, Phys. Rev. Lett. **114**, 067201 (2015).
[7] R. Valdés Aguilar, M. Mostovoy, A. B. Sushkov, C. L. Zhang, Y. J. Choi, S.-W. Cheong, and H. D. Drew, Phys. Rev. Lett. **102**, 047203 (2009).
[8] C. Lu, M. Wu, L. Lin, and J.-M. Liu, Natl. Sci. Rev. **6**, 653 (2019).
[9] R. D. Johnson, S. Nair, L. C. Chapon, A. Bombardi, C. Vecchini, D. Prabhakaran, A. T. Boothroyd, and P. G. Radaelli, Phys. Rev. Lett. **107**, 137205 (2011).
[10] K. Xu, J. S. Feng, Z. P. Liu, and H. J. Xiang, Phys. Rev. Appl. **9**, 044011 (2018).
[11] K. T. Kang, C. J. Roh, J. Lim, T. Min, J. H. Lee, K. Lee, T. Y. Lee, S. Kang, D. Seol, J. Kim, H. Ohta, A. Khare, S. Park, Y. Kim, S. C. Chae, Y. S. Oh, J. Lee, J. Yu, J. S. Lee, and W. S. Choi, Adv. Mater. **31**, 1808104 (2019).
[12] J. W. Kim, S. Y. Haam, Y. S. Oh, S. Park, S.-W. Cheong, P. A. Sharma, M. Jaime, N. Harrison, J. H. Han, G.-S. Jeon, P. Coleman, and K. H. Kim, Proc. Natl. Acad. Sci. USA **106**, 15573 (2009).
[13] K. Dunnett, J.-X. Zhu, N. A. Spaldin, V. Juričić, and A. V. Balatsky, Phys. Rev. Lett. **122**, 057208 (2019).
[14] Y. J. Choi, N. Lee, P. A. Sharma, S. B. Kim, O. P. Vajk, J. W. Lynn, Y. S. Oh, and S.-W. Cheong, Phys. Rev. Lett. **110**, 157202 (2013).
[15] J. M. Edge, Y. Kedem, U. Aschauer, N. A. Spaldin, and A. V. Balatsky, Phys. Rev. Lett. **115**, 247002 (2015).
[16] C. W. Rischau, X. Lin, C. P. Grams, D. Finck, S. Harms, J. Engelmayer, T. Lorenz, Y. Gallais, B. Fauque, J. Hemberger, and K. Behnia, Nat. Phys. **13**, 643 (2017).
[17] J. R. Arce-Gamboa and G. G. Guzmán-Verri, Phys. Rev. Mater. **2**, 104804 (2018).
[18] S. E. Rowley, L. J. Spalek, R. P. Smith, M. P. M. Dean, M. Itoh, J. F. Scott, G. G. Lonzarich, and S. S. Saxena, Nat. Phys. **10**, 367 (2014).
[19] A. Narayan, A. Cano, A. V. Balatsky, and N. A. Spaldin, Nat. Mater. **18**, 223 (2019).
[20] F. Schrettle, S. Krohns, P. Lunkenheimer, A. Loidl, E. Wulf, T. Yankova, and A. Zheludev, Phys. Rev. B **87**, 121105(R) (2013).
[21] D. M. Juraschek, M. Fechner, A. V. Balatsky, and N. A. Spaldin, Phys. Rev. Mater. **1**, 014401 (2017).
[22] R. Chen, J. F. Wang, Z. W. Ouyang, Z. Z. He, S. M. Wang, L. Lin, J. M. Liu, C. L. Lu, Y. Liu, C. Dong, C. B. Liu, Z. C. Xia, A. Matsuo, Y. Kohama, and K. Kindo, Phys. Rev. B **98**, 184404 (2018).
[23] Z. W. Ouyang, Y. C. Sun, J. F. Wang, X. Y. Yue, R. Chen, Z. X. Wang, Z. Z. He, Z. C. Xia, Y. Liu, and G. H. Rao, Phys. Rev. B **97**, 144406 (2018).
[24] R. Chen, H. J. Hu, Z. Qu, Y. R. Song, Q. K. Lei, C. B. Liu, Y. S. Tang, C. L. Wang, Z. Z. He, Z. W. Ouyang, K. Zhang, Y. Qiu, C. Dong, and J. F. Wang, J. Phys.: Condens. Matter **35**, 205801 (2023).
[25] J. J. Cao, Z. W. Ouyang, X. C. Liu, T. T. Xiao, Y. R. Song, J. F. Wang, Y. Ishii, X. G. Zhou, and Y. H. Matsuda, Phys. Rev. B **106**, 184409 (2022).
[26] R. Chen, J. F. Wang, Z. W. Ouyang, M. Tokunaga, A. Y. Luo, L. Lin, J. M. Liu, Y. Xiao, A. Miyake, Y. Kohama, C. L. Lu, M. Yang, Z. C. Xia, K. Kindo, and L. Li, Phys. Rev. B **100**, 140403(R) (2019).
[27] Z. He, J.-I. Yamaura, Y. Ueda, and W. Cheng, Phys. Rev. B **79**, 092404 (2009).
[28] Z. He, J.-I. Yamaura, Y. Ueda, and W. Cheng, J. Solid State Chem. **182**, 2526 (2009).
[29] I. Urcelay-Olabarria, E. Ressouche, Z. Wang, Y. Skourski, V. Y. Ivanov, Y. F. Popov, G. P. Vorobev, A. M. Balbashov, N. Qureshi, J. L. García-Muñoz, V. Skumryev, and A. A. Mukhin, Phys. Rev. B **96**, 104435 (2017).
[30] N. Abe, K. Taniguchi, S. Ohtani, T. Takenobu, Y. Iwasa, and T. Arima, Phys. Rev. Lett. **99**, 227206 (2007).
[31] S. Chikara, J. Singleton, J. Bowlan, D. A. Yarotski, N. Lee, H. Y. Choi, Y. J. Choi, and V. S. Zapf, Phys. Rev. B **93**, 180405(R) (2016).
[32] Y. Kohama, C. Marcenat, T. Klein, and M. Jaime, Rev. Sci. Instrum. **81**, 104902 (2010).
[33] L. Yin, Z. W. Ouyang, J. F. Wang, X. Y. Yue, R. Chen, Z. Z. He, Z. X. Wang, Z. C. Xia, and Y. Liu, Phys. Rev. B **99**, 134434 (2019).
[34] See Supplemental Material at http://link.aps.org/supplemental/10.1103/PhysRevB.108.224405 for more details.

[35] Y. J. Liu, J. F. Wang, Z. Z. He, C. L. Lu, Z. C. Xia, Z. W. Ouyang, C. B. Liu, R. Chen, A. Matsuo, Y. Kohama, K. Kindo, and M. Tokunaga, Phys. Rev. B **97**, 174429 (2018).

[36] J. Beilsten-Edmands, S. J. Magorrian, F. R. Foronda, D. Prabhakaran, P. G. Radaelli, and R. D. Johnson, Phys. Rev. B **94**, 144411 (2016).

[37] W. H. Ji, L. Yin, W. M. Zhu, C. M. N. Kumar, C. Li, H.-F. Li, W. T. Jin, S. Nandi, X. Sun, Y. Su, T. Brückel, Y. Lee, B. N. Harmon, L. Ke, Z. W. Ouyang, and Y. Xiao, Phys. Rev. B **100**, 134420 (2019).

[38] A. A. Aczel, Y. Kohama, M. Jaime, K. Ninios, H. B. Chan, L. Balicas, H. A. Dabkowska, and G. M. Luke, Phys. Rev. B **79**, 100409(R) (2009).

[39] H. Ryll, K. Kiefer, C. Rüegg, S. Ward, K. W. Krämer, D. Biner, P. Bouillot, E. Coira, T. Giamarchi, and C. Kollath, Phys. Rev. B **89**, 144416 (2014).

[40] J.-S. Xiang, C. Chen, W. Li, X.-L. Sheng, N. Su, Z.-H. Cheng, Q. Chen, and Z.-Y. Chen, Sci. Rep. **7**, 44643 (2017).

[41] M. Jaime, V. F. Correa, N. Harrison, C. D. Batista, N. Kawashima, Y. Kazuma, G. A. Jorge, R. Stein, I. Heinmaa, S. A. Zvyagin, Y. Sasago, and K. Uchinokura, Phys. Rev. Lett. **93**, 087203 (2004).

[42] V. Zapf, M. Jaime, and C. D. Batista, Rev. Mod. Phys. **86**, 563 (2014).

[43] E. C. Samulon, Y. Kohama, R. D. McDonald, M. C. Shapiro, K. A. Al-Hassanieh, C. D. Batista, M. Jaime, and I. R. Fisher, Phys. Rev. Lett. **103**, 047202 (2009).

[44] G. S. Uhrig and H. J. Schulz, Phys. Rev. B **54**, R9624 (1996).

[45] S. Kimura, K. Kakihata, Y. Sawada, K. Watanabe, M. Matsumoto, M. Hagiwara, and H. Tanaka, Nat. Commun. **7**, 12822 (2016).

[46] M. Garst and A. Rosch, Phys. Rev. B **72**, 205129 (2005).

[47] L. Zhu, M. Garst, A. Rosch, and Q. Si, Phys. Rev. Lett. **91**, 066404 (2003).